

## Nature helps

### Toward bioinspired bactericidal nanopatterns

Ganjan, Mahya; Modaresifar, Khashayar; Ligeon, Manon R.O.; Kunkels, Lorenzo B.; Tümer, Nazli; Angeloni, Livia; Hagen, Kees; Otten, Linda G.; Hagedoorn, Peter Leon; Apachitei, Iulian

#### DOI

[10.1002/admi.201900640](https://doi.org/10.1002/admi.201900640)

#### Publication date

2019

#### Document Version

Final published version

#### Published in

Advanced Materials Interfaces

#### Citation (APA)

Ganjan, M., Modaresifar, K., Ligeon, M. R. O., Kunkels, L. B., Tümer, N., Angeloni, L., Hagen, K., Otten, L. G., Hagedoorn, P. L., Apachitei, I., Fratila-Apachitei, L. E., & Zadpoor, A. A. (2019). Nature helps: Toward bioinspired bactericidal nanopatterns. *Advanced Materials Interfaces*, 6(16), Article 1900640. <https://doi.org/10.1002/admi.201900640>

#### Important note

To cite this publication, please use the final published version (if applicable).  
Please check the document version above.

#### Copyright

Other than for strictly personal use, it is not permitted to download, forward or distribute the text or part of it, without the consent of the author(s) and/or copyright holder(s), unless the work is under an open content license such as Creative Commons.

#### Takedown policy

Please contact us and provide details if you believe this document breaches copyrights.  
We will remove access to the work immediately and investigate your claim.

# Nature Helps: Toward Bioinspired Bactericidal Nanopatterns

Mahya Ganjian,\* Khashayar Modaresifar,\* Manon R. O. Ligeon, Lorenzo B. Kunkels, Nazli Tümer, Livia Angeloni, Cornelis W. Hagen, Linda G. Otten, Peter-Leon Hagedoorn, Iulian Apachitei, Lidy E. Fratila-Apachitei, and Amir A. Zadpoor

Development of synthetic bactericidal surfaces is a drug-free route to the prevention of implant-associated infections. Surface nanotopographies with specific dimensions have been shown to kill various types of bacterial strains through a mechanical mechanism, while regulating stem cell differentiation and tissue regeneration. The effective ranges of dimensions required to simultaneously achieve both aims are in the <200 nm range. Here, a nanoscale additive manufacturing (=3D printing) technique called electron beam induced deposition (EBID) is used to fabricate nanopillars with reproducible and precisely controlled dimensions and arrangements that are within those effective ranges (i.e. a height of 190 nm, a diameter of 80 nm, and an interspacing of 170 nm). When compared to the flat surface, the nanopatterned surfaces show a significant bactericidal activity against both *Escherichia coli* and *Staphylococcus aureus* (with respective killing efficiencies of  $97 \pm 1\%$  and  $36 \pm 5\%$ ). Direct penetration of nanopatterns into the bacterial cell wall leads to the disruption of the cell wall and cell death. The more rigid cell wall of *S. aureus* is consistent with the decreased killing efficiency. These findings support the development of nanopatterns with precisely controlled dimensions that are capable of killing both Gram-negative and Gram-positive bacteria.

## 1. Introduction

While the increased life expectancy is leading to increased numbers of surgical replacement of orthopedic implants, further increasing risk of implant-associated infection (IAI) is among the main causes of the failure of those implants.<sup>[1]</sup> Opportunistic pathogens including different types of bacteria are able to attach to and grow on the implant surface, eventually forming a biofilm, which is less susceptible to antibiotics and cannot be easily cleared by the host immune system.<sup>[2]</sup> This phenomenon hinders the function of the implant and results in significant morbidity and/or mortality.<sup>[3]</sup>

Different techniques have been proposed for prevention of bacterial attachment to the implant surface and/or for killing the bacteria upon contact with the surface.<sup>[4]</sup> While the majority of non-adherent surfaces are unfavorable for the attachment of both bacterial and host cells, they are not of much utility in this

case. That is because attachment and growth of host cells on the implant surface is a crucial step in the osseointegration process. One therefore needs surfaces that can selectively kill bacteria while supporting the growth and proliferation of host cells.<sup>[5]</sup> Consequently, there has been a surge in the efforts aimed at developing contact-killing surfaces with such properties. Noncytotoxic bactericidal surfaces primarily work on the basis of a chemical or physical killing mechanism. As chemical methods usually deliver antibiotics,<sup>[6,7]</sup> bactericidal metallic nanoparticles such as silver,<sup>[8–10]</sup> or other antibacterial agents,<sup>[11]</sup> their long-term widespread use may lead to the development of bacterial resistance against the delivered agents.<sup>[12–14]</sup>


On the other hand, surface topographies at the nano- and sub-micrometer scales have been shown to be capable of killing bacteria through mechanical pathways.<sup>[15,16]</sup> Indeed, several nanotopographical features found in nature, exhibit bactericidal behavior and have inspired the development of an alternative approach to common chemical methods.<sup>[17,18]</sup> A great number of these surface nanotopographies are distinguished by their highly controlled spatial arrangements of their nanoscale features.<sup>[19]</sup> Recent advances in micro- and nanofabrication techniques have enabled researchers to replicate some of these

M. Ganjian, K. Modaresifar, M. R. O. Ligeon, L. B. Kunkels, Dr. N. Tümer, Dr. L. Angeloni, Dr. I. Apachitei, Dr. L. E. Fratila-Apachitei, Prof. A. A. Zadpoor

Department of Biomechanical Engineering  
Faculty of Mechanical, Maritime, and Materials Engineering  
Delft University of Technology  
Mekelweg 2, 2628CD Delft, The Netherlands  
E-mail: m.ganjian@tudelft.nl; k.modaresifar@tudelft.nl

Dr. C. W. Hagen  
Department of Imaging Physics  
Faculty of Applied Sciences  
Delft University of Technology  
Lorentzweg 1, 2628CJ Delft, The Netherlands

Dr. L. G. Otten, Dr. P.-L. Hagedoorn  
Department of Biotechnology  
Faculty of Applied Sciences  
Delft University of Technology  
Van der Maasweg 9, 2629HZ Delft, The Netherlands

 The ORCID identification number(s) for the author(s) of this article can be found under <https://doi.org/10.1002/admi.201900640>.

© 2019 The Authors. Published by WILEY-VCH Verlag GmbH & Co. KGaA, Weinheim. This is an open access article under the terms of the Creative Commons Attribution-NonCommercial License, which permits use, distribution and reproduction in any medium, provided that the original work is properly cited and is not used for commercial purposes.

DOI: 10.1002/admi.201900640

naturally occurring nanopatterns (e.g., spinules of gecko skin) on synthetic materials or to develop new nanopatterns with desired design parameters such as height (depth), diameter, and interspacing.<sup>[20,21]</sup>

Reactive ion etching (RIE), hydrothermal treatment, anodizing, electron beam lithography (EBL), and nanoimprint lithography (NIL) can be considered as the most commonly used methods to create nanopatterns. However, the size range that these methods are able to produce and the controllability of the process highly differs from one technique to another.<sup>[19]</sup> In order to systematically investigate the effects of nanopattern design parameters on the bactericidal properties, it is crucial to use a technique which allows the user to control each single design parameter independently from all others while being able to precisely and reproducibly fabricate feature sizes below 100 nm.<sup>[22]</sup> Electron beam induced deposition (EBID) is a nanoscale additive manufacturing (=3D printing) method, which enables the user to approach feature sizes in the range of a few nanometers<sup>[23]</sup> by dissociating precursor molecules

using a focused electron beam (**Figure 1a**). Precursor molecules dissociate into two parts, a volatile and a nonvolatile part.<sup>[22]</sup> The nonvolatile part remains on the substrate and creates a deposited layer, while the volatile part desorbs and is evacuated.<sup>[24]</sup> Some studies have shown the EBID potential to create arrays of nanopillars with dimensions of a single nanometer<sup>[22]</sup> as well as complex 2D and 3D shapes.<sup>[25–32]</sup>

The effective range for the design parameters of surface nanopatterns (in the shape of pillars) in which the bacteria could be mechanically killed in the absence of any antibacterial agents (i.e., the range between 100 and 900 nm for the height; 20 and 207 nm for the diameter; 9 nm and 380 nm for the interspacing; and the aspect ratio higher than 2) has been recently reported.<sup>[19]</sup> In the specific cases of *Escherichia coli* and *Staphylococcus aureus* as model organisms representing Gram-negative and Gram-positive bacteria, the reported ranges of dimensions of nanopillars to induce bactericidal behavior are as follows: diameters of 70–100 nm for *S. aureus* and 70–80 nm for *E. coli*, heights of 100–900 nm for *S. aureus*, and 180–300 nm for

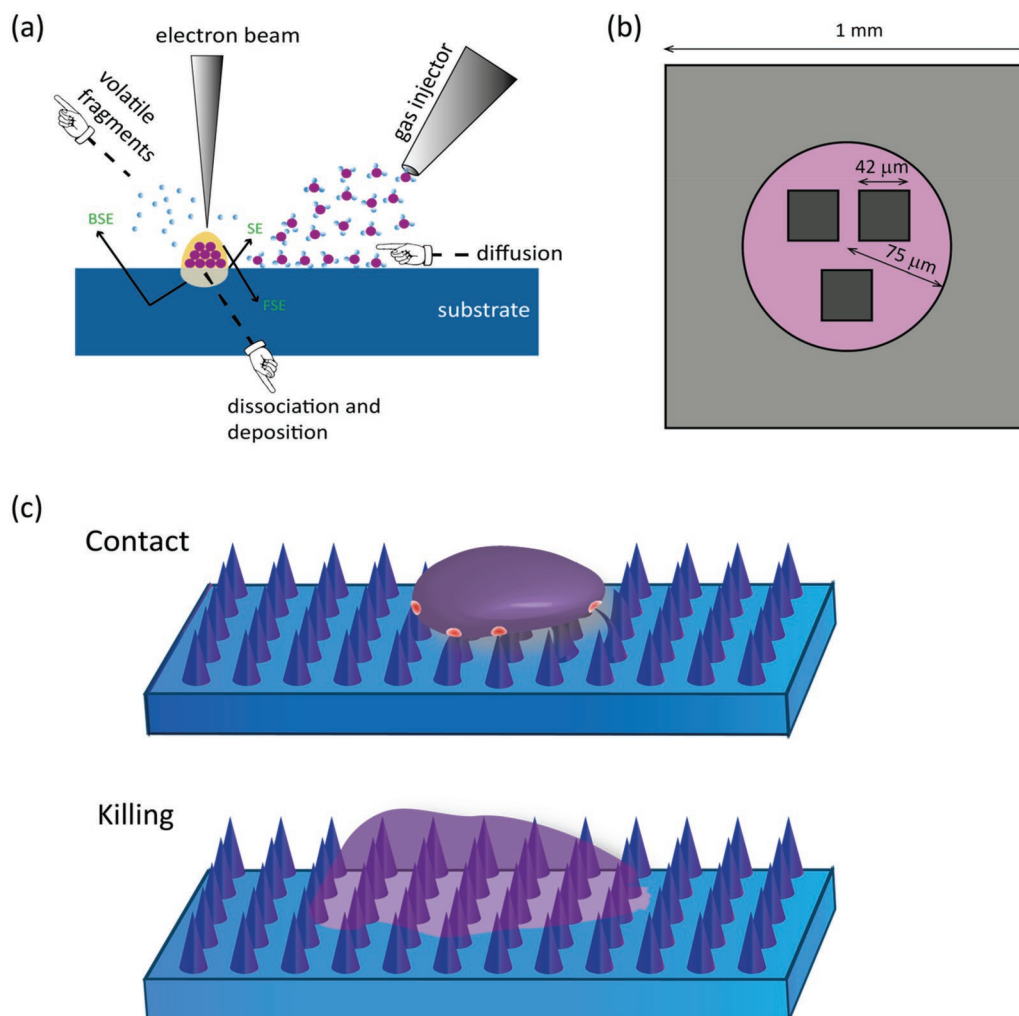


**Figure 1.** a) Schematic representation of the EBID method; b) sample design: dark gray indicates the patterned area, the pink area is close to the patterns, and the light gray area is far from the patterns; c) a schematic drawing demonstrating the fate of bacteria residing on nanopatterns including deformation on the nanopatterns upon contact and being sunk on the nanopatterns due to the penetration of nanopillars into the bacterial cell wall.

*E. coli*, and interspaces of 60–200 nm for *S. aureus* and 60–380 nm for *E. coli*.<sup>[19]</sup> To simultaneously target both Gram-positive and Gram-negative bacteria, we chose the following approximate dimensions: height = 190 nm, diameter = 80 nm, and interspace = 170 nm. It is, nevertheless, worth noting that the bactericidal behavior of nanopatterns is not only dependent on the nanopatterns dimensions but also on the type of the bacterial strains and their initial attachment to the surface.<sup>[19,33,34]</sup> A bacterial cell is likely to deform or sink into the nanopatterns due to the penetration of the nanopillars into the bacterial cell wall (Figure 1c). To the best of our knowledge, the present study is the first to use EBID as a powerful tool to fabricate nanopatterns with precisely controlled dimensions chosen from the above-mentioned range in order to have a nanopatterned surface with high killing efficiency against both Gram-negative and Gram-positive bacteria.

## 2. Results

### 2.1. Characterization of Nanopatterns

Three patterned areas ( $42 \times 42 \mu\text{m}^2$ ) were fabricated on each sample (Figure 1b) under the previously mentioned conditions. Nanopatterns were produced in the shape of pillars (similar to a droplet-shaped structure) (Figure 2f). The nanopillars had a mean height of 186 nm (SD 8 nm), a base diameter of 75 nm (SD 5 nm), a tip diameter of 21 nm (SD 3 nm), and an interpillar spacing of 170 nm (Figure 2). The nanopillar density was 36 pillars per  $\mu\text{m}^2$  (Figure 2c,h). The chemical composition of the EBID deposited material included  $\approx 15.5\%$  Pt,  $\approx 73.4\%$  C, and  $\approx 8.7\%$  O (Figure 2g). The result of the water contact angle measurement on the surface of Pt–C showed the hydrophilicity of the surface with a contact angle of  $59 \pm 2^\circ$  (inset of Figure 2g). Applying the Cassie–Baxter wettability model showed a hydrophobic contact angle of  $169 \pm 0.1^\circ$  for the nanopatterned surface.

### 2.2. Bactericidal Activity of Nanopatterns

*E. coli* cells exhibited their normal rod-shaped morphology on flat silicon samples (Figure 3a,b) and the mean percentage of damaged/dead cells was 8.0% (SD 6.4%) on the control surfaces (Figure 5). Similar to previous studies,<sup>[35]</sup> the live cells had an average length of 2.6  $\mu\text{m}$  (SD 0.7  $\mu\text{m}$ ) and a width of 808 nm (SD 107 nm) (Figure 3a,b). On the other hand, *E. coli* cells were found extremely deformed on the nanopatterned surfaces (Figure 3e,f) with substantial amounts of disrupted bacterial cell wall and remnant cellular fragments on the nanopatterned areas (Figure 3c–e). The killing efficiency was  $97.0 \pm 1.2\%$  for *E. coli* cells on the nanopatterned surfaces. The length and width of the cells on the nanopatterned surfaces could not be determined due to the drastic deformations and disruptions of the bacterial cells (Figure 3f).

Similarly, *S. aureus* cells had a normal coccoid-shaped morphology and size<sup>[36]</sup> on the Si control surfaces with an average diameter of  $\approx 790$  nm (SD 66 nm), and no bacterial cell was found damaged or dead (Figure 4a,b). The damaged cells,

mostly sunk on the nanopillars, showed a squashed morphology and the penetration of the nanopillars into the bacterial cell wall could be clearly seen (Figure 4d,f). Additionally, bending of the nanopillars underneath the bacterial cells was observed and leftovers of bacterial components were also found on some of the nanopillars (Figure 4e,f). The killing efficiency of the nanopatterns for *S. aureus* cells was  $36.5 \pm 4.7\%$  (Figure 5). Furthermore, the bactericidal efficiency of Pt–C surface against *E. coli* and *S. aureus* was significantly lower than the nanopatterned surface ( $p < 0.0001$  and  $p < 0.01$ , respectively) (Figure 5).

## 3. Discussion

Designing multibiofunctional surfaces to selectively influence the behavior of mammalian cells and bacteria is of high current interest and importance for the development of implant materials as well as being a formidable challenge given the substantial differences between mammalian cells and bacteria in sensing and responding to surfaces.<sup>[37]</sup> Some of the naturally occurring nanopatterned surfaces (e.g., gecko skin, cicada wings, dragonfly wings) have shown bactericidal properties while they are not cytotoxic (Figure 6).<sup>[17,33,38–42]</sup>

When it comes to designing orthopedic implants, the holy grail would be having surfaces which simultaneously kill bacteria and promote osteogenesis (or osteogenic differentiation of stem cells). The main contribution of this study was application of an ultrafine nanoscale 3D printing process with a resolution of a few nanometers to create nanopatterns with reproducible and precisely controlled dimensions that exhibit bactericidal behavior against both Gram-negative and Gram-positive bacteria. The dimensions of the nanopatterns produced in this study are within the bactericidal range found in literature and close to some of the naturally occurring bactericidal surfaces (Figure 6).<sup>[19]</sup> The vast majority of commonly used nanofabrication techniques do not allow control over individual dimension of such nanostructures independently from the other dimensions. EBID makes it feasible to produce specific controllable dimensions at the nanoscale, with a resolution comparable or better than EBL.<sup>[22]</sup> Additionally, there is no need for a mask or other chemical wet processes. These characteristics make EBID an ideal method for producing nanopatterns that are required for performing systematic studies to determine which exact dimensions of the nanopatterns result in maximum bactericidal activity while promoting osteogenic differentiation of the host cells. EBID uses a precursor gas (trimethyl(methylcyclopentadienyl)-platinum(IV) in this study) to write directly on the substrate. In the EBID process, the precursor gas molecules dissociate on the substrate under the electron beam.<sup>[43]</sup> The main components of the deposited material in this study were platinum and carbon. The platinum percentage can vary from 8.9% to 16.8% depending on the beam current, deposition time, and electron dosage.<sup>[44]</sup>

The nanopatterned surface showed a high bactericidal efficiency against *E. coli* where almost all the bacterial cells were sunk on the nanopillars with the cell components leaked out and a distorted morphology. However, the nanopatterns could not kill *S. aureus* as efficiently as *E. coli*. Considering that the bactericidal activity of the nanopatterns is physical in nature



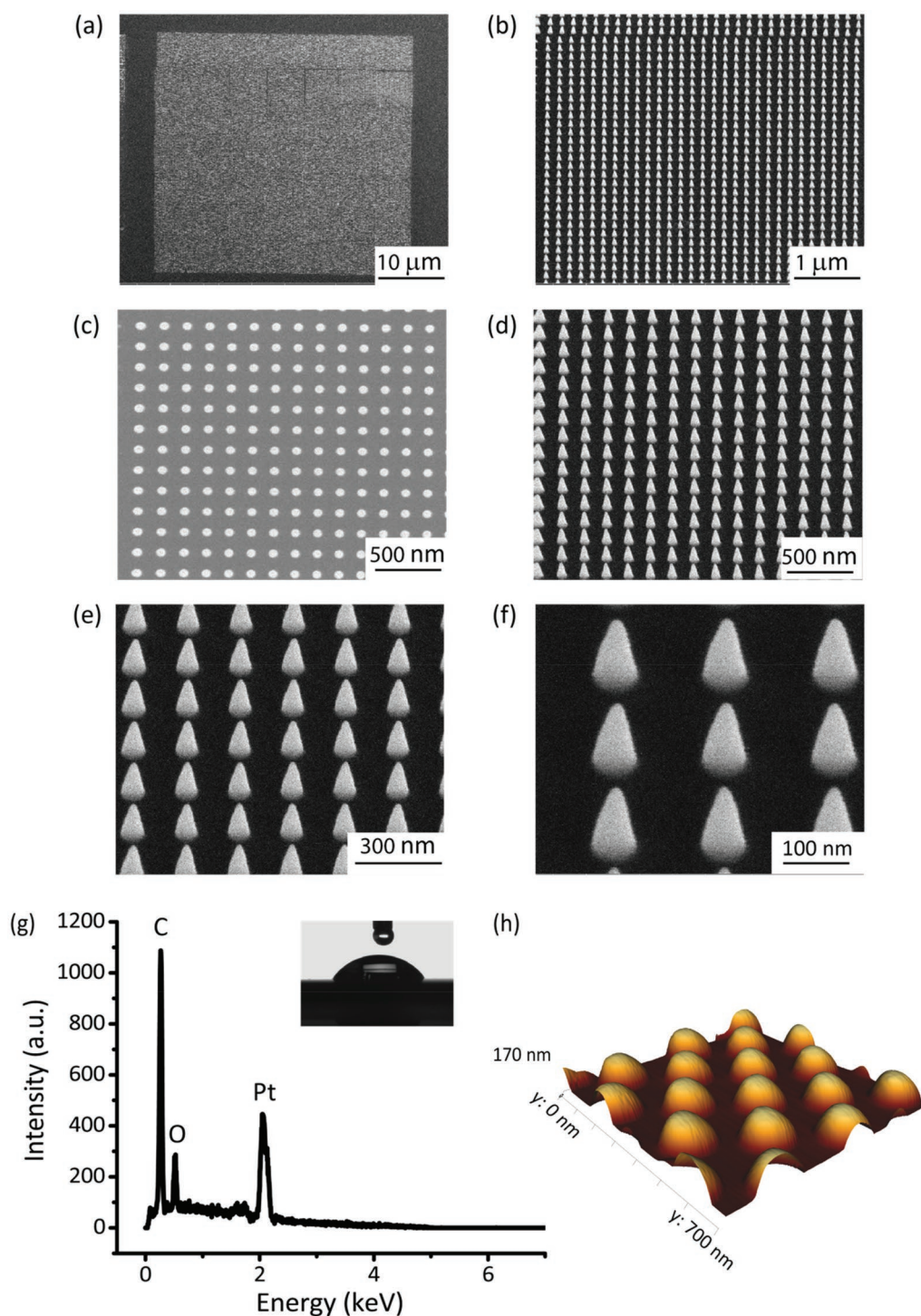


**Figure 2.** a–f) SEM images of nanopillars produced by EBID at different magnifications: a,c) top view and b,d,e,f) 35° tilted view. g) EDX characterization of Pt-C deposited structure, the inset shows the water contact angle on the flat Pt-C surface. h) AFM imaging showing a 3D overview of the nanopillars.

(corroborated by the results of Pt-C flat surface), the difference between the bactericidal efficiency against *E. coli* and *S. aureus* could be explained by the more rigid and thicker cell wall of *S. aureus* which requires higher forces to be ruptured.<sup>[17,38,45]</sup> Bending of the nanopillars beneath the bacteria is consistent with this hypothesis (Figure 4e,f). Other differences

between Gram-negative and Gram-positive bacteria such as the size and morphology could also affect the bactericidal efficiency.<sup>[46]</sup> Moreover, as remnant fragments of *S. aureus* were observed on the nanopatterns (Figure 4e), one could speculate that the bacteria had found the surface unfavorable for adhesion and moved away from the surface. This hypothesis has

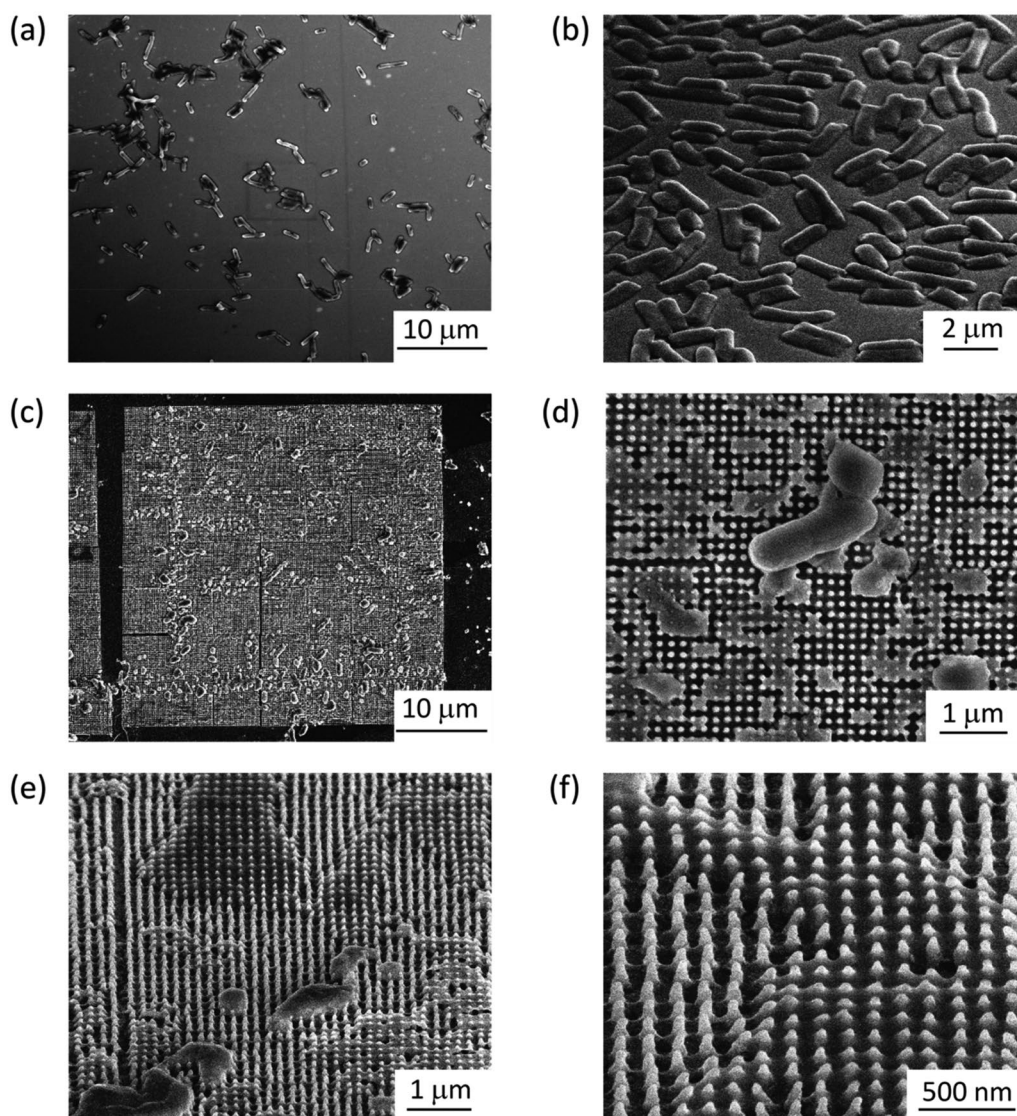


**Figure 3.** SEM images of *E. coli* bacteria on the control Si surface: a) top overview and b) 50° tilted view. SEM images of *E. coli* bacteria on the nano-patterned surface after 18 h incubation: c) top overview, d) damaged bacteria from top view, e) damaged bacteria from 50° tilted view, and f) bacteria totally sunk into the nanopatterns (50° tilted view).

been previously introduced in the literature.<sup>[41]</sup> If a number of bacteria have moved away from the surface, the antibacterial activity that includes the bactericidal effects and prevention of bacterial adhesion to the surface, might have been stronger than what could be concluded from the SEM images alone. Due to the small size of the patterned areas (compared to the whole samples' surface) which could be fabricated by EBID, other methods of antibacterial activity assessment such as live/dead staining and CFU enumeration<sup>[47]</sup> were not applicable. Nevertheless, previous studies have shown that bacteria with similar irregular/damaged morphologies are equivalent to the dead bacteria in those mentioned methods.<sup>[48,49]</sup>

While the direct penetration of high aspect-ratio nanopatterns into the bacterial cell wall and their consequent disruption is considered the main bactericidal mechanism of nanopatterned surfaces, many other factors have been proposed to play

important roles in the bactericidal potential of nanopatterned surfaces.<sup>[19]</sup> For instance, the uniformity of the nanopatterns,<sup>[50]</sup> their compaction<sup>[51]</sup> and density<sup>[52]</sup> on the surface, and surface wettability<sup>[19]</sup> have been shown to affect the bactericidal activity. In this regard, theoretical studies with a mechanistic point of view have previously shown that the interspacing and the diameter of the nanopillars could be the determining factors for applying the highest force and imposing the highest degree of stretching and deformation, and ultimately, death in bacteria.<sup>[53]</sup> Therefore, more systematic studies are needed to improve the bactericidal efficiency of nanopatterns against more resistant bacteria such as methicillin resistant *S. aureus*. Moreover, studying the behavior of mammalian cells on such nanopatterns is required to better visualize and tag the exact overlapping range of bactericidal and osteogenic nanopatterns. So far, an overlap between the bactericidal and osteogenic ranges can



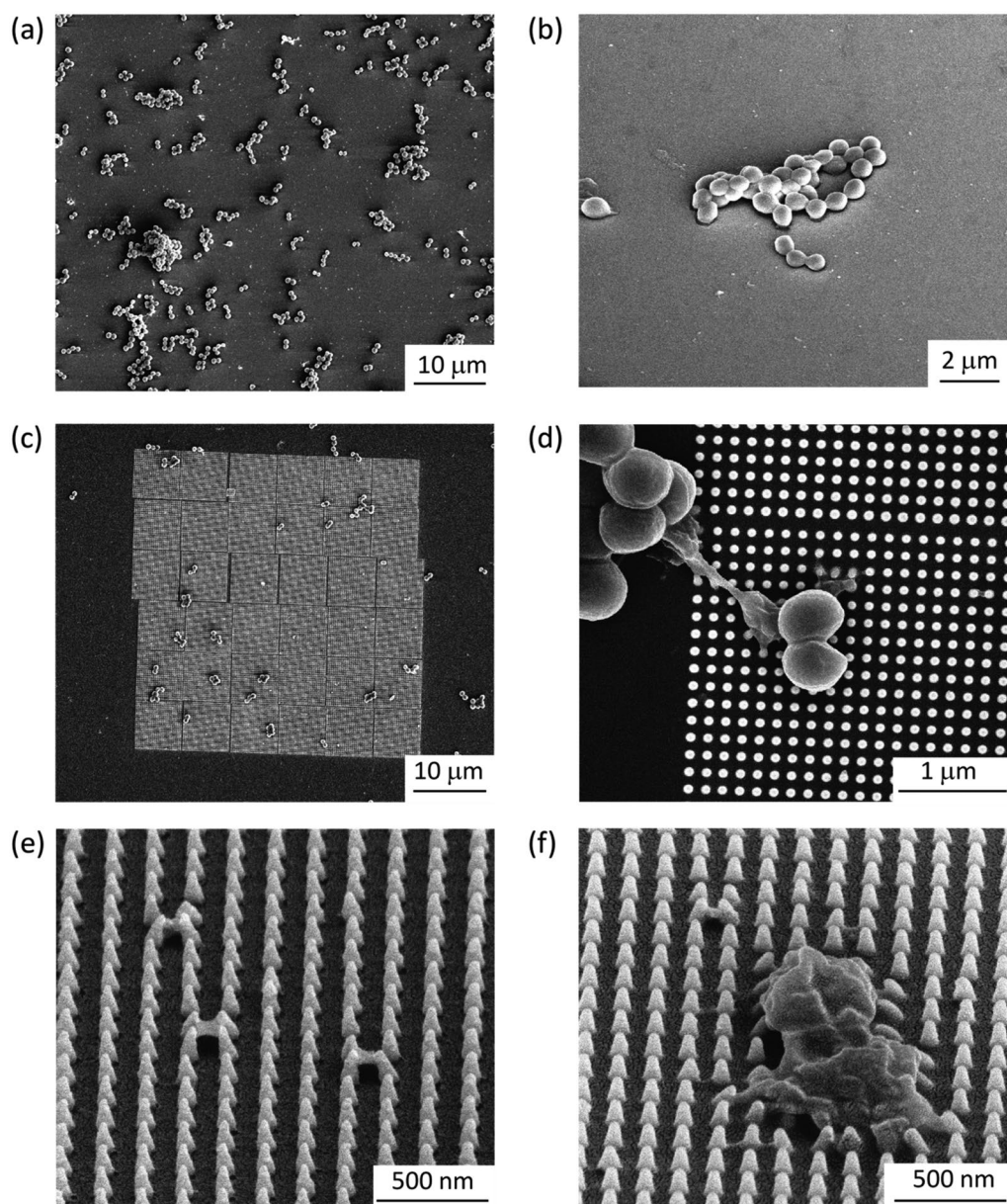


**Figure 4.** SEM images of *S. aureus* bacteria on the control Si surface: a) top overview and b) 50° tilted view. SEM images of *S. aureus* bacteria on the nanopatterned surface: c) top overview, d) two healthy and one dead bacteria on the pattern from top view, e) the remnant fragments of the bacteria on the nanopillars, and f) two dead bacteria on the nanopatterns from 50° tilted view.

already be pictured based on the data available in the literature (Figure 7).<sup>[19,54–59]</sup> The nanopatterns produced in this study are positioned inside the overlap area of these two important types of behavior, implying that they are likely to exhibit osteogenic properties as well. It is therefore important to further assess their osteogenic properties in future studies. Indeed, more studies on the osteogenic behavior of nanopatterned surfaces are required to more accurately define the boundaries of the osteogenic range.

Although EBID enables fabrication of nanopatterns with arbitrary shapes and accurate controllable dimensions, which is ideal for systematic studies, upscaling the patterned area is still challenging. It took 6.5 h to produce each of the  $42 \times 42 \mu\text{m}^2$

patterned areas, check the dimensions, and refocus again to have exactly the same nanostructures. To create surfaces that are suitable for further experiments with mammalian cells such as mesenchymal stem cells (MSCs) culture, it is necessary to enlarge the patterned area, for example to  $3 \times 3 \text{ mm}^2$  which could be achieved by further developments of the process. One approach would be to use parallel electron beam induced deposition using a multibeam scanning electron microscope, which enables patterning the desired area using several parallel beams (e.g.,  $14 \times 14$  beams to expose a larger area and reduce the required deposition time to a few hours<sup>[60]</sup>). Another method, which has a comparably higher throughput, higher resolution, and lower cost is using EBID patterns as a mask stamp

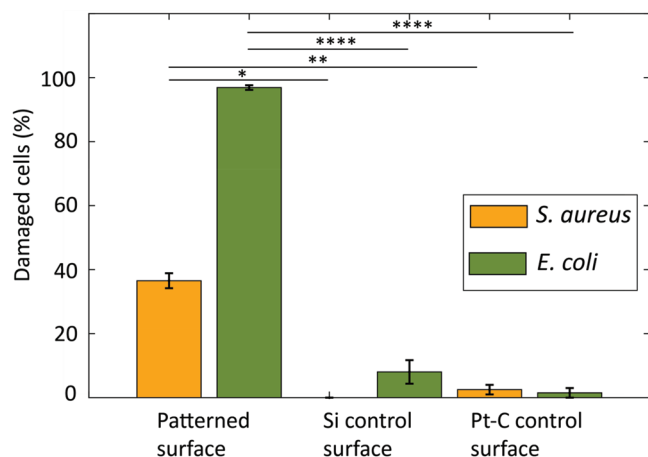


**Figure 5.** Quantitative characterization of the percentage of damaged *E. coli* and *S. aureus* bacterial cells on nanopatterned, Si control, and Pt-C control surfaces (\* $p < 0.05$ , \*\* $p < 0.01$ , \*\*\* $p < 0.001$ , and \*\*\*\* $p < 0.0001$ ). The killing efficiency was not affected by the chemical composition of the surface and the number of damaged/dead cells was significantly higher on the nanopatterned surface.

for step and repeat nanoimprint lithography (NIL). There are two major NIL methods: UV NIL and thermal NIL. For UV step and repeat NIL, one needs to deposit the desired nanopatterns on a substrate that is highly transmissive to deep UV (e.g., fused silica,<sup>[61]</sup> glass substrate,<sup>[62]</sup> etc.). The thermal step and repeat NIL is another technique to enlarge the nanopatterned area. Si is the preferred stamp material for thermal NIL due to its high elastic modulus, mechanical strength, and thermal expansion coefficient.<sup>[63]</sup> Transferring EBID nanopatterns composed of the precursor molecules into Si substrate as the NIL stamp, is the first step for this technique, which needs to be done by RIE.<sup>[64,65]</sup> In both NIL methods, the following step after

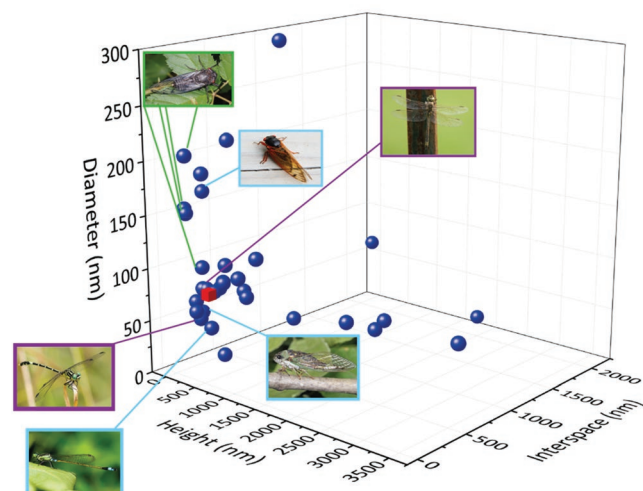


**Figure 6.** The dimensions of the bactericidal nanopatterns found in the literature. The nanopattern produced for this study (represented as the red square) had dimensions close to the dimension range of naturally occurring nanopatterns. The images of insects with green and blue frames are reprinted from wikipedia.org and stock.adobe.com, respectively, with permission. The images with purple frame are taken by Roos Coy (www.therebedragonflies.com.au) and reprinted with permission.

preparing a nanopatterned stamp is bringing the stamp in contact with the desired substrate that should have been covered by imprint polymer inside a nanoimprint machine and applying a constant pressure. After the required time, the pressure is released and the user can separate the stamp from the polymer and move it to pattern the next desired area. The final step is etching the residual layer of the imprint polymer and the substrate using RIE. Regardless of the chosen upscaling technique, the underlying EBID technology is the key to achieving reproducible and precisely controlled nanopatterns and is therefore recommended for future studies.

## 4. Conclusion

In order to develop a bactericidal surface suitable for fabrication of orthopedic implants, we used EBID to create nanopatterns with dimensions within the bactericidal range and comparable to nanopatterns found in nature in terms of height and diameter. The nanopatterns were produced in the shape of pillars with a height of  $\approx 190$  nm, a diameter of 80 nm, and an interspace of 170 nm. The nanopatterns were found to mechanically rupture the cell wall of *E. coli* and *S. aureus* and showed a significantly higher bactericidal activity as compared to the nonpatterned surfaces and flat surfaces coated with the same material as the pillars. However, the bactericidal efficiency for *S. aureus* was significantly lower than *E. coli*, which could be explained by the differences in the characteristics of Gram-negative and Gram-positive bacteria such as the cell wall thickness and stiffness. Further investigations are required to determine the exact killing mechanism, the role of different factors involved in that process, and the possible osteogenic activity, since the dimensions of the current nanopatterns are within the osteogenic range. Although EBID is a very powerful technique to have control over all of the dimensions of the nanopatterns in the fabrication process, the challenge of upscaling the patterned area while reducing the writing time is yet to be overcome. This

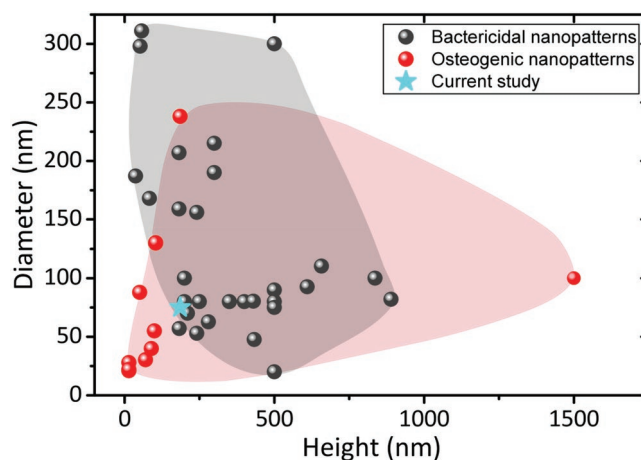


**Figure 7.** Comparison of the dimensions (diameter and height) of nanopillars found in the literature displaying bactericidal and osteogenic activities. This graph illustrates that the nanopattern studied here is within the area where nanopatterns possess both bactericidal and osteogenic properties.



is crucial for further experiments on mammalian cells, which are bigger in size than bacterial cells. Such an approach would open the way for the development of nanopatterns with simultaneous bactericidal and osteogenic potential that could be translated to clinical use in the future.

## 5. Experimental Section

**Nanopatterns Design, Fabrication, and Characterization:** Double-sided polished 4 in. (diameter = 10.16 cm) silicon wafers (thickness =  $525 \pm 25 \mu\text{m}$ , p-type) were diced into  $1 \times 1 \text{ cm}^2$  samples and cleaned with nitric acid. A streamfile was designed to create nanopillars with a square arrangement possessing the approximate dimensions of 190, 80, and 170 nm for their height, base diameter, and center-to-center spacing, respectively. A Nova Nano Lab 650 Dual Beam system (FEI company, OR, USA) equipped with EBID and scanning electron microscopy (SEM) was used to create three nanopatterned areas of  $42 \times 42 \mu\text{m}^2$  on each sample (Figure 1b). Trimethyl(methylcyclopentadienyl)-platinum(IV),  $(\text{CH}_3\text{C}_5\text{H}_4)\text{Pt}(\text{CH}_3)_3$ ,  $\text{MeCpPtIVMe}_3$ , or  $\text{C}_9\text{H}_{18}\text{Pt}$  was used as the precursor gas and EBID was performed in the electron limited regime and at a working distance of 5 mm with 17.8 kV as the electron beam voltage and 0.60 nA as the beam current. The background vacuum of the system was  $8.82 \times 10^{-7}$  mbar and the EBID process started at  $2.33 \times 10^{-6}$  mbar (as the minimum reachable chamber pressure after opening the gas injection system and leaving the sample for 2 h inside the chamber). The writing strategy was single dot exposure, using stream files generated by a MATLAB (MathWorks, US) code. The resulting nanopatterns were characterized by SEM. The height, base diameter, and tip diameter were measured for sixty different pillars per sample by using  $35^\circ$  tilted SEM images. The center-to-center spacing was also measured from the top view images. The mean and standard deviation of the measurements were calculated. The chemical composition of the specimens was characterized using an energy-dispersive X-ray spectroscopy (EDX) analysis performed inside an SEM (Helios NanoLab 600i dualbeam, FEI, Hillsboro, USA) on a Pt/C deposited structure with 1000 nm as the diameter and 192 nm as the height, using an image with  $\times 16\,000$  magnification acquired with an accelerating voltage of 5 kV. Nanopatterns were also imaged using atomic force microscopy (AFM) with a Dimension FastScan AFM (Bruker, Billerica, USA) in the ScanAsyst mode with a scan rate of 0.96 Hz and a FastScan-A probe having a nominal spring constant of  $18 \text{ N m}^{-1}$  and nominal tip radius of 5 nm. To measure the water contact angle of the nanopatterns, a thin layer of Pt-C was initially deposited on a set of silicon wafers to identify the static contact angle of Pt-C material ( $\theta_0$ ) by a drop shape analyzer (DSA 100, Kruss, Hamburg, Germany) using deionized water. A volume of  $2 \mu\text{L}$  liquid with a falling rate of  $1667 \mu\text{L min}^{-1}$  was placed on the surface using a syringe. The contact angle figure was recorded 5 s after the droplet had rested on the surface. The reported value for the measurement is the average contact angle within 30 s after the whole volume of the droplet touched the substrate. Since the nanopatterned area is too small compared to the water droplet, its contact angle was measured indirectly using the Cassie–Baxter wettability model, assuming that air was trapped between the nanopillars.<sup>[66,67]</sup> The following equation gives the Cassie–Baxter contact angle ( $\theta_c$ )

$$\cos(\theta_c) = \phi(\cos(\theta_0) + 1) - 1 \quad (1)$$

Here,  $\phi$  and  $\theta_0$  are the solid fraction (the ratio between the tip area of the nanopillar and the projected surface area) and the contact angle of the flat Pt–C surface, respectively. The solid fraction was calculated as follows

$$\phi = \frac{\pi d^2}{4i^2} \quad (2)$$

where  $d$  represents the tip diameter of the nanopillar and  $i$  is the interspacing of the nanopillars.

**Bacterial Growth Conditions:** Gram-negative bacteria *Escherichia coli* (K12 strain) (BEI Resources, VA, USA) and Gram-positive bacteria *Staphylococcus aureus* (RN0450 strain) (BEI Resources, VA, USA) were used to investigate the bactericidal activity of nanopatterned surfaces. *E. coli* and *S. aureus* were grown on Lysogeny broth (LB) (BD Life Sciences, CA, USA) and brain heart infusion (BHI) (Sigma-Aldrich, MO, USA) agar plates at  $37^\circ\text{C}$  overnight. Precultures of both bacteria cells were prepared by inoculating a single colony in 10 mL autoclaved LB/BHI liquid medium, shaken at 140 rpm at  $37^\circ\text{C}$ . The bacterial cells were collected at their logarithmic stage of growth and their optical density at 600 nm wavelength ( $\text{OD}_{600}$ ) in the medium solution was adjusted at a value of 0.05 ( $55.1 \times 10^6 \text{ CFU mL}^{-1}$ ) and 0.1 ( $61.6 \times 10^6 \text{ CFU mL}^{-1}$ ) for *E. coli* and *S. aureus*, respectively.

**Evaluation of Bactericidal Properties:** The nanopatterned areas of the surface and the surrounding nonpatterned areas ( $75 \mu\text{m}$ ) (Figure 1b) were considered as the study (triplicate) and control groups in the bacterial studies, respectively. A thin layer of Pt–C was also deposited on a set of silicon wafers to distinguish the bactericidal effect of nanopatterns from those of the deposition material itself. Samples were immersed in 70% ethanol and subsequently dried exposed to UV light for 20 min in a sterile flow cabinet prior to addition of the bacterial culture. For each type of bacteria, a sample containing three nanopatterned areas was inoculated with 1 mL of bacterial suspension in a 24-well plate (Cell Star, Germany). The samples were then incubated at  $37^\circ\text{C}$  for 18 h. Subsequently, the adhered bacteria were fixed for SEM imaging using a fixation solution containing 4% formaldehyde (Sigma-Aldrich, Missouri, USA) and 1% glutaraldehyde (Sigma-Aldrich, Missouri, USA) in  $10 \times 10^{-3} \text{ M}$  phosphate buffer. The samples were then washed with MilliQ water and 50%, 70%, and 96% ethanol, respectively, and eventually, soaked in hexamethyldisilazane (HMDS) (Sigma-Aldrich, MO, USA) for 30 min and air-dried.

A thin layer of gold was sputtered on the samples and SEM images were acquired at various magnifications and tilt angles for each sample. The total number of bacteria adhered to the surface was counted manually from the SEM images. Due to the small patterned area on the surface, it was not feasible to use other assessment methods like live/dead staining and colony forming unit (CFU) counting. The damaged/dead bacteria were distinguished by a drastic change in their morphology compared to a normal live cell or by observing disruption of their cell wall. The bactericidal efficiency of nanopatterned and nonpatterned areas was determined by dividing the number of damaged/dead bacteria to the total number of bacteria in those regions.

**Statistical Analysis:** To assess if there is a significant difference between the killing efficiency of different surfaces (i.e., silicon surface, Pt–C surface, and nanopatterned surface), an analysis of variance was conducted using the one-way ANOVA test followed by a post hoc analysis. Depending on the results of Levene's test for the equality of variance, we made a decision about applying Bonferroni test (in case that the resultant  $p$ -value of Levene's test is higher than 0.05), or Games–Howell test (in case that the resultant  $p$ -value of Levene's test is less than 0.05). Mean  $\pm$  standard deviation for the bactericidal measurements were provided. The statistical analysis was conducted using IBM SPSS Statistics 23 Software and a  $p$ -value less than 0.05 was considered to be statistically significant.

## Acknowledgements

M.G., K.M., and M.R.O.L. contributed equally to this work. This research has received funding from the European Research Council under the ERC grant agreement no. 677575.

## Conflict of Interest

The authors declare no conflict of interest.

## Keywords

antibacterial effects, biomimetics, nanoscale additive manufacturing, surface nanopatterns

Received: April 10, 2019

Revised: May 9, 2019

Published online: June 6, 2019

- [1] W. Zimmerli, A. Trampuz, P. E. Ochsner, *N. Engl. J. Med.* **2004**, 351, 1645.
- [2] C. R. Arciola, D. Campoccia, L. Montanaro, *Nat. Rev. Microbiol.* **2018**, 16, 397.
- [3] J. M. Steckelberg, D. R. Osmon, *Prosthetic Joint Infections*, American Society of Microbiology, Washington, DC, USA **2000**.
- [4] J. Hasan, R. J. Crawford, E. P. Ivanova, *Trends Biotechnol.* **2013**, 31, 295.
- [5] Y. Wang, G. Subbiahdoss, J. Swartjes, H. C. van der Mei, H. J. Busscher, M. Libera, *Adv. Funct. Mater.* **2011**, 21, 3916.
- [6] S. Bakhshandeh, Z. Gorgin Karaji, K. Lietaert, A. C. Fluit, C. E. Boel, H. C. Vogely, T. Vermonden, W. E. Hennink, H. Weinans, A. A. Zadpoor, *ACS Appl. Mater. Interfaces* **2017**, 9, 25691.
- [7] J. Hirschfeld, E. M. Akinoglu, D. C. Wirtz, A. Hoerauf, I. Bekeredjian-Ding, S. Jepsen, E.-M. Haddouti, A. Limmer, M. Giersig, *Nanomedicine* **2017**, 13, 1587.
- [8] M. Croes, S. Bakhshandeh, I. van Hengel, K. Lietaert, K. van Kessel, B. Pouran, B. van der Wal, H. Vogely, W. Van Hecke, A. Fluit, *Acta Biomater.* **2018**, 81, 315.
- [9] I. A. van Hengel, M. Riool, L. E. Fratila-Apachitei, J. Witte-Bourma, E. Farrell, A. A. Zadpoor, S. A. Zaat, I. Apachitei, *Biomaterials* **2017**, 140, 1.
- [10] S. Amin Yavari, L. Loozen, F. L. Paganelli, S. Bakhshandeh, K. Lietaert, J. A. Groot, A. C. Fluit, C. Boel, J. Alblas, H. C. Vogely, *ACS Appl. Mater. Interfaces* **2016**, 8, 17080.
- [11] X. J. Loh, *J. Mol. Eng. Mater.* **2017**, 5, 1740001.
- [12] A. Elbourne, R. J. Crawford, E. P. Ivanova, *J. Colloid Interface Sci.* **2017**, 508, 603.
- [13] A. Panáček, L. Kvítek, M. Smékalová, R. Večeřová, M. Kolář, M. Röderová, F. Dyčka, M. Šebela, R. Pucek, O. Tomanec, *Nat. Nanotechnol.* **2018**, 13, 65.
- [14] M. C. Enright, D. A. Robinson, G. Randle, E. J. Feil, H. Grundmann, B. G. Spratt, *Proc. Natl. Acad. Sci. USA* **2002**, 99, 7687.
- [15] S. Ghosh, S. Niu, M. Yankova, M. Mecklenburg, S. M. King, J. Ravichandran, R. K. Kalia, A. Nakano, P. Vashishta, P. Setlow, *Sci. Rep.* **2017**, 7, 17768.
- [16] D. P. Linklater, S. Juodkazis, S. Rubanov, E. P. Ivanova, *ACS Appl. Mater. Interfaces* **2017**, 9, 29387.
- [17] J. Hasan, H. K. Webb, V. K. Truong, S. Pogodin, V. A. Baulin, G. S. Watson, J. A. Watson, R. J. Crawford, E. P. Ivanova, *Appl. Microbiol. Biotechnol.* **2013**, 97, 9257.
- [18] I. Izquierdo-Barba, J. M. García-Martín, R. Álvarez, A. Palmero, J. Esteban, C. Pérez-Jorge, D. Arcos, M. Vallet-Regí, *Acta Biomater.* **2015**, 15, 20.
- [19] K. Modaresifar, S. Azizian, M. Ganjian, L. E. Fratila-Apachitei, A. A. Zadpoor, *Acta Biomater.* **2018**, 83, 29.
- [20] D. W. Green, K. K.-H. Lee, J. A. Watson, H.-Y. Kim, K.-S. Yoon, E.-J. Kim, J.-M. Lee, G. S. Watson, H.-S. Jung, *Sci. Rep.* **2017**, 7, 41023.
- [21] M. N. Dickson, E. I. Liang, L. A. Rodriguez, N. Vollereaux, A. F. Yee, *Biointerphases* **2015**, 10, 021010.
- [22] W. F. Van Dorp, B. Van Someren, C. W. Hagen, P. Kruit, P. A. Crozier, *Nano Lett.* **2005**, 5, 1303.
- [23] M.-K. Seo, H.-G. Park, J.-K. Yang, J.-Y. Kim, S.-H. Kim, Y.-H. Lee, *Opt. Express* **2008**, 16, 9829.
- [24] G. Gazzadi, S. Frabboni, C. Menozzi, L. Incerti, *Microelectron. Eng.* **2008**, 85, 1166.
- [25] W. Van Dorp, C. W. Hagen, *J. Appl. Phys.* **2008**, 104, 10.
- [26] S. Janbaz, N. Noordzij, D. S. Widayati, C. W. Hagen, L. E. Fratila-Apachitei, A. A. Zadpoor, *Sci. Adv.* **2017**, 3, eaao1595.
- [27] T. Bret, I. Utke, P. Hoffmann, *Microelectron. Eng.* **2005**, 78, 307.
- [28] T. Bret, I. Utke, P. Hoffmann, M. Abourida, P. Doppelt, *Microelectron. Eng.* **2006**, 83, 1482.
- [29] R. Winkler, F.-P. Schmidt, U. Haselmann, J. D. Fowlkes, B. B. Lewis, G. Kothleitner, P. D. Rack, H. Plank, *ACS Appl. Mater. Interfaces* **2016**, 9, 8233.
- [30] J. D. Fowlkes, R. Winkler, B. B. Lewis, A. Fernandez-Pacheco, L. Skoric, D. Sanz-Hernandez, M. G. Stanford, E. Mutunga, P. D. Rack, H. Plank, *ACS Appl. Nano Mater.* **2018**, 1, 1028.
- [31] J. D. Fowlkes, R. Winkler, B. B. Lewis, M. G. Stanford, H. Plank, P. D. Rack, *ACS Nano* **2016**, 10, 6163.
- [32] L. Keller, M. Huth, *Beilstein J. Nanotechnol.* **2018**, 9, 2581.
- [33] K. Nowlin, A. Boseman, A. Covell, D. Lajeunesse, *J. R. Soc., Interface* **2015**, 12, 20140999.
- [34] T. Diu, N. Faruqi, T. Sjöström, B. Lamarre, H. F. Jenkinson, B. Su, M. G. Ryadnov, *Sci. Rep.* **2014**, 4, 7122.
- [35] O. Pierucci, *J. Bacteriol.* **1978**, 135, 559.
- [36] L. Harris, S. Foster, R. Richards, *Eur. Cells Mater.* **2002**, 4, 39.
- [37] K. Anselme, P. Davidson, A. Popa, M. Giazgon, M. Liley, L. Ploux, *Acta Biomater.* **2010**, 6, 3824.
- [38] E. P. Ivanova, J. Hasan, H. K. Webb, V. K. Truong, G. S. Watson, J. A. Watson, V. A. Baulin, S. Pogodin, J. Y. Wang, M. J. Tobin, *Small* **2012**, 8, 2489.
- [39] V. K. Truong, N. M. Geeganagamage, V. A. Baulin, J. Vongsivut, M. J. Tobin, P. Luque, R. J. Crawford, E. P. Ivanova, *Appl. Microbiol. Biotechnol.* **2017**, 101, 4683.
- [40] S. M. Kelleher, O. Habimana, J. Lawler, B. O'Reilly, S. Daniels, E. Casey, A. Cowley, *ACS Appl. Mater. Interfaces* **2015**, 8, 14966.
- [41] C. D. Bandara, S. Singh, I. O. Afara, A. Wolff, T. Tesfamichael, K. Ostrikov, A. Oloyede, *ACS Appl. Mater. Interfaces* **2017**, 9, 6746.
- [42] G. S. Watson, D. W. Green, L. Schwarzkopf, X. Li, B. W. Cribb, S. Myhra, J. A. Watson, *Acta Biomater.* **2015**, 21, 109.
- [43] J. Wnuk, S. Rosenberg, J. Gorham, W. Van Dorp, C. Hagen, D. Fairbrother, *Surf. Sci.* **2011**, 605, 257.
- [44] A. Botman, M. Hesselberth, J. Mulders, *Microelectron. Eng.* **2008**, 85, 1139.
- [45] S. Pogodin, J. Hasan, V. A. Baulin, H. K. Webb, V. K. Truong, V. Boshkovikj, C. J. Fluke, G. S. Watson, J. A. Watson, R. J. Crawford, *Biophys. J.* **2013**, 104, 835.
- [46] E. Fadeeva, V. K. Truong, M. Stiesch, B. N. Chichkov, R. J. Crawford, J. Wang, E. P. Ivanova, *Langmuir* **2011**, 27, 3012.
- [47] J. Sjollem, S. A. Zaat, V. Fontaine, M. Ramstedt, R. Luginbuehl, K. Thevissen, J. Li, H. C. van der Mei, H. J. Busscher, *Acta Biomater.* **2018**, 70, 12.
- [48] E. P. Ivanova, J. Hasan, H. K. Webb, G. Gervinskas, S. Juodkazis, V. K. Truong, A. H. Wu, R. N. Lamb, V. A. Baulin, G. S. Watson, *Nat. Commun.* **2013**, 4, 2838.
- [49] D. Widayati, P.-L. Hagedoorn, L. Otten, M. Ganjian, N. Tumer, I. Apachitei, C. W. K. Hagen, L. Fratila-Apachitei, A. A. Zadpoor, *Nanotechnology* **2019**, 30.
- [50] L. E. Fisher, Y. Yang, M.-F. Yuen, W. Zhang, A. H. Nobbs, B. Su, *Biointerphases* **2016**, 11, 011014.
- [51] D. P. Linklater, H. K. D. Nguyen, C. M. Bhadra, S. Juodkazis, E. P. Ivanova, *Nanotechnology* **2017**, 28, 245301.
- [52] S. Wu, F. Zuber, K. Maniura-Weber, J. Brugger, Q. Ren, *J. Nanobiotechnol.* **2018**, 16, 20.

- [53] M. Mirzaali, I. Van Dongen, N. Tümer, H. Weinans, S. A. Yavari, A. Zadpoor, *Nanotechnology* **2018**, 29, 43LT02.
- [54] J.-H. Hwang, D.-H. Lee, M. R. Byun, A. R. Kim, K. M. Kim, J. I. Park, H. T. Oh, E. S. Hwang, K. B. Lee, J.-H. Hong, *Sci. Rep.* **2017**, 7, 3632.
- [55] T. Sjöström, L. E. McNamara, R. D. Meek, M. J. Dalby, B. Su, *Adv. Healthcare Mater.* **2013**, 2, 1285.
- [56] Z. Li, J. Qiu, L. Q. Du, L. Jia, H. Liu, S. Ge, *Mater. Sci. Eng.* **2017**, 76, 684.
- [57] L. E. McNamara, T. Sjöström, K. E. Burgess, J. J. Kim, E. Liu, S. Gordonov, P. V. Moghe, R. D. Meek, R. O. Oreffo, B. Su, *Biomaterials* **2011**, 32, 7403.
- [58] T. Sjöström, M. J. Dalby, A. Hart, R. Tare, R. O. Oreffo, B. Su, *Acta Biomater.* **2009**, 5, 1433.
- [59] G. M. de Peppo, H. Agheli, C. Karlsson, K. Ekström, H. Brisby, M. Lennerås, S. Gustafsson, P. Sjövall, A. Johansson, E. Olsson, *Int. J. Nanomed.* **2014**, 9, 2499.
- [60] P. Post, A. Mohammadi-Gheidari, C. Hagen, P. Kruit, *J. Vac. Sci. Technol., B: Nanotechnol. Microelectron.: Mater., Process., Meas., Phenom.* **2011**, 29, 06F310.
- [61] Y. Zhao, E. Berenschot, M. De Boer, H. Jansen, N. Tas, J. Huskens, M. Elwenspoek, *J. Micromech. Microeng.* **2008**, 18, 064013.
- [62] D. J. Resnick, S. Sreenivasan, C. G. Willson, *Mater. Today* **2005**, 8, 34.
- [63] L. J. Guo, *Adv. Mater.* **2007**, 19, 495.
- [64] H. Cao, Z. Yu, J. Wang, J. O. Tegenfeldt, R. H. Austin, E. Chen, W. Wu, S. Y. Chou, *Appl. Phys. Lett.* **2002**, 81, 174.
- [65] A. Notargiacomo, E. Giovine, L. Di Gaspare, *Microelectron. Eng.* **2011**, 88, 2710.
- [66] B. Bhushan, M. Nosonovsky, *Philos. Trans. R. Soc., A* **2010**, 368, 4713.
- [67] M. Sun, G. S. Watson, Y. Zheng, J. A. Watson, A. Liang, *J. Exp. Biol.* **2009**, 212, 3148.